

Electrical Equivalent Circuit Models for Brushless Doubly-Fed Induction Machines: A Review

Hamidreza Mosaddegh-Hesar, *Member, IEEE*, Xiaodong Liang, *Senior Member, IEEE*, Mohammad-Ali Salahmanesh, Salman Abdi, *Senior Member, IEEE* and Richard McMahon

Abstract--A Brushless Doubly-Fed Induction Machine (BDFIM) has wide application potential in wind turbines, industrial drives, small hydro power plants, power supply of ships, aircraft starters, and electric vehicles. In electric vehicles, a BDFIM offers a robust structure without needing permanent magnet materials, slip-rings, and brushes, which makes it particularly suitable for heavy vehicles, such as buses, agriculture and construction vehicles, where the low power density of a BDFIM is of less significance compared to that in passenger cars. To effectively analyze and control a BDFIM in various applications, it is essential to develop its accurate electrical equivalent circuit models. This paper presents a comprehensive review on various electrical equivalent circuit models of BDFIMs in the literature with different level of complexity. A full order model is complex, but can represent the complete electrical behavior of a BDFIM. By simplifying the full order model and neglecting certain parameters, a reduced order model requires fewer state variables due to practical approximations. Dynamic behavior of BDFIMs under various operating conditions are demonstrated in the paper to showcase the effectiveness of these existing models. This review emphasizes the significance of electrical equivalent circuit models in the design, analysis and control of BDFIMs. Future research directions for the model refinement are recommended.

Index Terms-- Brushless doubly fed induction machine, electrical equivalent circuits, full order model, iron losses, magnetic saturation.

NOMENCLATURE

$\vec{v}, \vec{i}, \vec{\lambda}$	Voltage, current, flux vectors
T_e	Torque
P	Power
R	Winding resistance
L_l	Leakage inductance
L_m	Magnetizing inductance
L_{MpD}	D -axis component of power winding (PW) magnetizing inductance
L_{MpQ}	Q -axis component of PW magnetizing inductance
L_{McD}	D -axis component of control winding (CW) magnetizing inductance
L_{McQ}	Q -axis component of CW magnetizing inductance

L_{pDQ}	Cross-coupling inductance between D - and Q -axis of PW
L_{cDQ}	Cross-coupling inductance between D - and Q -axis of CW
L_{pD}	D - axis component of PW self-inductance
L_{pQ}	Q - axis component of PW self-inductance
L_{cD}	D - axis component of CW self-inductance
L_{cQ}	Q - axis component of CW self-inductance
p	Number of pole pair
N_r	Number of rotor loops (nests)
f	Frequency
ω_r	Synchronous rotor speed
ω_a	Arbitrary angular speed
ω_n	Natural synchronous speed
s	Derivative operator
Subscripts	
p, c, r	PW, CW, rotor
d, q	Arbitrary reference frame
m	Magnetizing

I. INTRODUCTION

WITH introduction of alternating current (AC) electric machines in the late 19th century, their speed control became a fundamental requirement. However, efficiently controlling the speed of AC machines across a wide operating range was a significant challenge. In 1897, Steinmetz in the United States and Görges in Germany developed a cascade control system [1] as a solution to achieve more flexible control of induction machines (IMs) with a cascade connection of two wound rotor IMs sharing a common shaft. In 1907, Hunt introduced a self-cascaded machine with a specially designed stator winding, featuring taps that could be connected to a rheostat for speed control or starting. Subsequently, researchers at the University of Bristol studied Hunt's machine and developed a unique rotor structure, known as the "nested loop," which is still prevalent in the modern brushless doubly fed induction machine (BDFIM) designs [2],[3]. Building upon the research conducted at Bristol University, Wallace, Li, and Spee at Oregon State University made significant advancements in the mid-1980s by investigating the use of two separated stator

This work was supported in part by Natural Science and Engineering Research Council of Canada (NSERC) Discovery Grant RGPIN-2016-04170 (Corresponding author: Xiaodong Liang).

Hamidreza Mosaddegh-Hesar and Xiaodong Liang are with the Department of Electrical and Computer Engineering, University of Saskatchewan, Saskatoon, SK, S7N 5A9, Canada (e-mail: pvt356@usask.ca, xil659@mail.usask.ca).

Mohammad-Ali Salahmanesh is with the Department of Electrical Engineering, Ferdowsi University of Mashhad, Mashhad, 9177948974, Iran (e-mail: m.salahmanesh@mail.um.ac.ir).

Salman Abdi is with the School of Engineering, University of East Anglia, Norwich NR4 7TJ, UK (e-mail: s.abdi-jalebi@uea.ac.uk, s.abdi.jalebi@gmail.com).

Richard McMahon is with University of Warwick, Coventry, CV4 7AL, UK (e-mail: r.mcmahon.1@warwick.ac.uk).

windings for self-cascaded doubly-fed induction machines [4]. By modifying the stator winding structure proposed by Hunt, they introduced what is now known as the BDFIM. The term “BDFIM” was first coined by Wallace in 1989, and the extensive research has been conducted on control, dynamics, and optimization of BDFIMs [5]-[9].

A BDFIM possesses remarkable characteristics by combining advantages of an IM and a synchronous machine. It operates efficiently with only a partially rated converter and enables the synchronous operation across a wide range of speed precisely by controlling the control winding's frequency. The brushless structure of a BDFIM ensures reliable operations and the fault tolerance, even in the event of converter failures [10]-[13]. BDFIMs can be used in wind turbines [15]-[18], industrial drives [19]-[22], small hydro power plants [23], power supply of ships [24], aircraft starters [25], and electric vehicles [26], [27]. For potential applications in electric vehicles, since a BDFIM does not need permanent magnet material, slip-rings and brushes, it can be implemented as near-wheel or wheel-hub direct traction drive. Multi-axle, multi-track vehicles are also suitable for BDFIMs, where each wheel in each operated axle is driven by its own motor. Furthermore, BDFIMs are particularly relevant for heavy vehicles, such as buses, agriculture and construction vehicles. Low power density of a BDFIM in these vehicles is of less significance compared to that in passenger cars, therefore, its cost effective materials and production, and its system level benefits due to power electronics, control and functional safety make the BDFIM a great choice in the transportation sector.

Studying the BDFIM's dynamic performance has been advanced by developing various mathematical models. The initial coupled circuit model, introduced by Wallace et al. [28],[29], provided valuable insights but had certain limitations. Specifically, the model did not account for the effects of the leakage inductance and saturation, and its applicability to a wide range of machines [30]. Analytically solving equations of this model, except for the standstill position, was not feasible due to the position-dependent mutual inductance matrices. To address these limitations, a two-axis model is derived from a coupled circuit model using a precise mathematical process in [6], so the characteristics of a BDFIM can be analyzed under steady state and dynamic conditions; separate three-phase windings are used in this model although a multi-tap single winding would be effectively the same under the modeling assumptions in [6]. In [31], Boger et al. generalized the model in [6] to any pole pair configurations by using an assumed stator and rotor configuration. They showed that a d-q transformation could be applied to a BDFIM. This transformation starts from an idealized machine, rather than an explicit transformation of a more general model. In [30], a BDFIM is viewed as two interconnected IMs, and a steady state equivalent circuit applicable to all modes of operations is formulated; this model has a complicated structure, making the analysis and control of a BDFIM difficult, and this complexity is further increased by considering iron loss effects. An over-simplified model, known as the “core model”, is proposed in [32] to analyze the steady state performance of a BDFIM in motoring and generating

modes; since magnetizing reactances and stator and rotor resistances are ignored in this core model, so it is not suitable for control purposes. To facilitate the analysis of a BDFIM, its steady state and dynamic models are simplified in [34]. Accordingly, its electromagnetic torque is broken down into induction and synchronous torque components. Through the electromagnetic torque analysis, simulations and experiments, it is found that the contribution of induction torque is negligible in practical applications. Therefore, simplifications are proposed in both steady state and dynamic models of BDFIMs, and BDFIM models become very similar to those of conventional doubly fed induction machines (DFIMs). These developments in mathematical modeling have significantly contributed to the understanding and analysis of BDFIMs' dynamic and steady-state behaviors. Analytical models also play a crucial role in predicting the machine performance during the design stage prior to construction.

One important factor to consider in the design and optimization of electrical machines is iron losses in the core, as iron losses play a significant role in the overall losses of an electric machine. For instance, in standard IMs, iron losses represent approximately 20% of the total losses on average [35]. It is recognized that neglecting iron losses during the vector control can lead to errors in the orientation angle of an IM [36]. BDFIMs tend to have higher iron losses than conventional IMs at the same capacity. This is primarily attributed to spatial harmonic distortions in the air-gap, a non-uniform distribution of the magnetic field, and operations that deviate from the synchronous speed of both stator fields [37]-[40]. Several models are proposed to consider iron losses in BDFIMs [41]-[44]. Ref. [41] presents a novel hysteresis model based on the scalar Preisach model for the stator iron of a BDFIM; this model assesses how rotational characteristics of magnetic fields in a BDFIM affect iron losses through 2-D time-stepping finite element (FE) analysis and experimental data from a prototype D160 BDFM. In [42], magnetic field characteristics in BDFIMs are investigated, and a new iron loss formulation is proposed by considering the rotational field and harmonic effects in the iron loss prediction. In [43], analytical models are presented specifically for iron losses in BDFIMs, but no equivalent circuits are developed to evaluate the effect of iron losses. Building upon similarities between BDFIMs and conventional IMs, a simple model for iron losses in BDFIMs is introduced in [44], which incorporates separate resistances on the power winding (PW) and control winding (CW) sides to determine iron losses for each stator winding (these resistance values are obtained through optimization).

Considering iron losses in BDFIMs, a steady-state equivalent circuit model is presented in [45] that includes four resistances: the PW's iron loss resistance, the rotor's iron loss resistance referred to the PW side, the CW's iron loss resistance, and the rotor's iron loss resistance referred to the CW side. This model provides a comprehensive representation of iron losses in BDFIMs. The model in [45] is further improved in [46] by deriving analytical expressions for the iron loss components related to each stator winding, and a steady-state model that considers iron losses in BDFIMs is proposed. In [47], the iron

loss modeling in a space vector equivalent circuit of BDFMs in a stationary reference frame is proposed. The torque equation is derived based on this model, and the impact of neglecting iron losses is demonstrated in the speed, torque, and input power waveforms. To simplify the complexity of the full order model, a reduced order model is developed in [48] while considering iron losses. This reduced order model neglects the direct cross-coupling between the stator and rotor's magnetic fields and introduces a practical method to calculate iron losses in BDFIMs with respect to frequency variations. In [49], dynamic modeling in an arbitrary reference frame is utilized to incorporate iron losses and saturation effects of the main flux in a two-axis model of BDFIMs. This model includes terms representing the cross-saturation effect to enhance accuracy. Taking into account the close relationship between the torque and the power, the torque equation is derived considering iron losses and magnetic saturation based on the electrical input power's expression.

Fig. 1 illustrates the evolution of the BDFIM's electric modeling. Initially, the electric equivalent circuit (EEC) took the form of a coupled-circuit model, which later progressed into various configurations. Although attempts to model BDFIMs can be traced back to the late 20th century, a significant breakthrough occurred with the introduction of a steady-state full order model by Roberts in 2004 [30]. This model served as the foundation for subsequent models in this field. This paper aims to offer a comprehensive overview of electrical equivalent circuit models developed for BDFIMs. The primary motivation behind conducting this review is to provide a broad and detailed insight into existing models, while evaluating their practicality, implementation, and accuracy. The importance of this review lies in its ability to facilitate advancements in BDFIMs research and development by understanding and analyzing strengths and weaknesses of these electrical equivalent circuit models. By examining various proposed models, researchers can identify the most suitable models for practical applications and address any limitations or challenges associated with the models' implementation. By consolidating the knowledge and insights gained from existing models, this review contributes to the progress of BDFIMs design, control, and performance optimization. To compare and analyze different models, several factors including mathematical formulation, nonlinear effects, complexity or simplicity are considered in this paper.

II. BDFIMs STRUCTURE

A BDFIM has two sets of balanced three-phase windings with the different number of poles wound on a single common stator frame (Fig. 2a). The first winding is known as the PW and is connected to the grid directly, and the majority of power exchange between the machine and the grid occurs through this winding. The second winding is called the CW and a partially rated back-to-back converter connects the CW to the grid. This converter enables the control over the rotor speed, the torque, and the reactive power of the PW. To prevent the direct magnetic coupling between the PW and the CW in a BDFIM, it is necessary that PW and CW windings have a different number of pole pairs [50]. To minimize the unbalanced magnetic pull

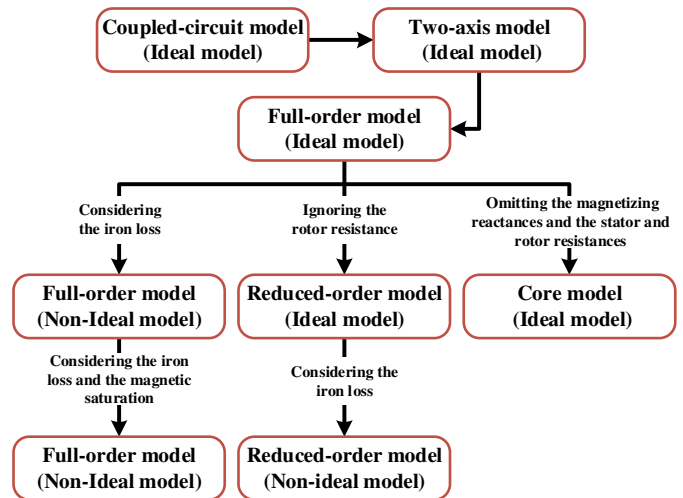


Fig. 1. A classification of electric equivalent circuits (EECs) of BDFIMs.

(UMP) on the rotor, the difference between the number of pole pairs of the two stator windings should be larger than one [51].

In [30], general guidelines are provided for selecting the number of poles. One winding should have an even number of pole pairs, while the other winding should have an odd number of pole pairs. Alternatively, both windings can have even numbers of pole pairs, as long as the ratio between the two sets of pole pairs is not an odd number. If the ratio of pole pairs is a multiple of three, both windings can have odd numbers of pole pairs. It is important to highlight that, when implementing the parallel winding design, it is crucial to exercise caution to prevent a direct coupling between the PW and the CW [52].

The rotor of a BDFIM features a unique cage structure known as the “nested loop”, and consists of multiple poles or nests (Fig. 2(b)). Each nest comprises a set of short-circuited concentric loops. The total number of nests is equal to the sum of pole pair numbers of the stator windings. Nested-loop rotors are used extensively in BDFIMs, but may not be suitable for large machines [53]. There are several advances on the basic version of the nested loop rotor. Two optimized rotors, a bar cage rotor and a nested-loop rotor, are developed in [53].

The loop number in the rotor of a BDFIM is determined by harmonic contents of the magnetomotive force and the permissible flux density in the rotor. Also, practicalities related to preferred stator and rotor slot number combinations do make some contributions to the torque and reduce harmonics.

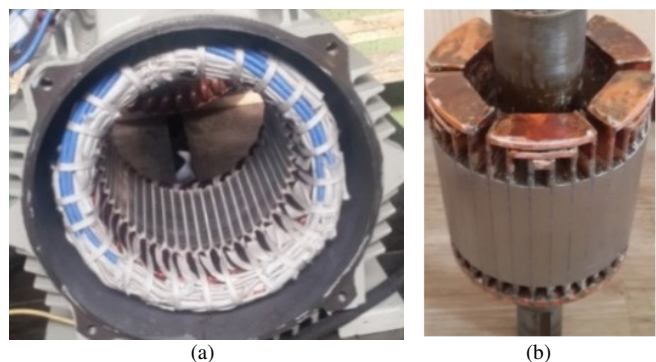


Fig. 2. The BDFIM prototype: (a) Stator, (b) Nested-loop rotor (three loops in each nest) [54].

In a BDFIM, when one stator winding, either the PW or the CW, is connected to a power source, while the other stator winding remains open-circuited, the machine operates as an IM with p_p or p_c pole pairs, respectively. This scenario occurs during a converter failure and is known as the “induction mode”. In this mode, the machine exhibits similar characteristics to a standard IM with a compromised performance. On the other hand, if the non-supplied stator winding is short-circuited, the machine behaves as a cascaded IM. A cascade IM, formed by combining machines with p_p and p_c pole pairs, exhibits characteristics similar to an IM with $(p_p + p_c)$ pole pairs. This mode, known as the “cascade induction mode”, is typically used during starting and acceleration towards the synchronous speed. Both the induction mode and the cascade induction mode are asynchronous modes of operations, where the shaft speed depends on the machine load and the power supply frequency.

However, the synchronous mode is a desirable mode of operations for BDFIMs, and the speed is determined by the PW and CW’s frequencies. In this mode, the majority of power exchange between the machine and the grid occurs through the PW, and the CW only processes a fraction of the power, depending on the speed deviation from the synchronous speed.

III. ELECTRIC MODELING OF BDFIMs

The modeling of BDFIMs has been a significant focus since their introduction, as the study of machine behaviors and the development of control structures are based on their models. The steady-state full order model presented by Roberts et al. has served as the foundation for various models, including the core model, the full order model with iron losses, the reduced order model, the reduced order model with iron losses, and the full order model considering iron losses and magnetic saturation. The reduced order model offers a solution to a complex

structure of the full order model by reducing the number of electrical state variables, making the modeling and control of BDFIMs similar to that of DFIMs. Compared to the core model, the reduced order model provides a better approximation of the full order model by neglecting direct cross coupling. The core model, on the other hand, is a simplified version of the full order model by omitting the magnetizing reactance, as well as the stator and rotor resistances. These different modeling approaches provide varying levels of complexity and accuracy, allowing researchers and engineers to choose the most suitable model for their specific analysis and control design needs.

A. Full Order Model

A BDFIM can be understood as the combination of two distinct IMs that are interconnected within a common frame. The equivalent electric circuit for the BDFIM is derived from the single-phase equivalent circuit of each individual IM. Each machine comprises a wound rotor with a specific number of pole pairs, as depicted in Fig. 3. Note that each circuit has its own corresponding slip value. When the rotors of the two machines are interconnected, the single-phase steady-state equivalent circuit of the BDFIM can be referenced to the PW side, neglecting factors, such as iron losses and magnetic saturation, as shown in Fig. 4. The slips of the PW and CW are denoted as s_p and s_c and represented by

$$s_i \triangleq (\omega_i - p_i \omega_r) / p_i \omega_r, \quad i = p, c \quad (1)$$

In the synchronous mode, the rotor speed is independent of the applied torque and can be expressed by

$$\omega_r = (\omega_1 + \omega_2) / (p_1 + p_2) \quad (2)$$

If the CW is fed by a DC source ($\omega_2 = 0$), the rotor will rotate at a speed known as the “natural speed”. The law of conservation of energy is used to derive the torque equation of the full order model under steady state operations. For this purpose, Eqs. (3) and (4) are obtained from Fig. 4.

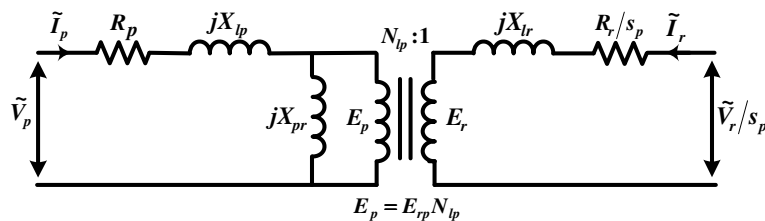


Fig. 3. Single-phase steady-state equivalent circuit of the IM [30].

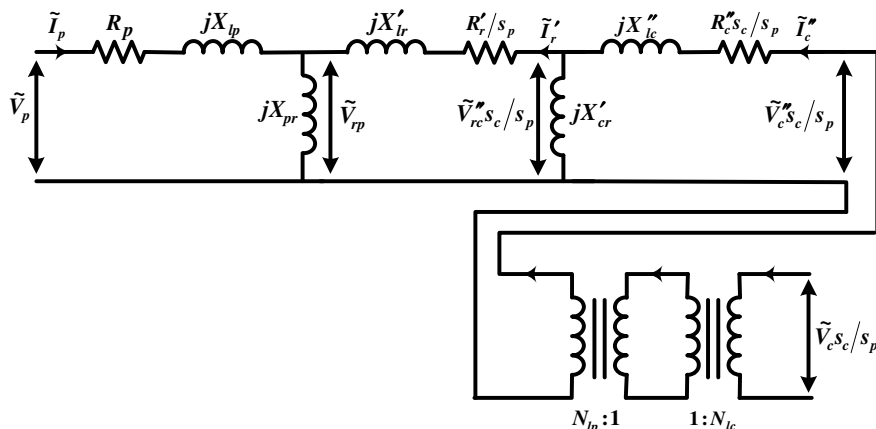


Fig. 4. Single-phase steady-state equivalent circuit of the BDFIM referred to the PW side [30].

$$3\Re\{\tilde{V}_p \tilde{I}_p^*\} + 3s_c/s_p \Re\{\tilde{V}_c \tilde{I}_c^*\} = 3R_p |\tilde{I}_p|^2 + 3R_r/s_p |\tilde{I}_r|^2 + 3R_c s_c/s_p |\tilde{I}_c|^2 \quad (3)$$

$$3\Re\{\tilde{V}_p \tilde{I}_p^*\} + 3\Re\{\tilde{V}_c \tilde{I}_c^*\} = 3R_p |\tilde{I}_p|^2 + 3R_r |\tilde{I}_r|^2 + 3R_c |\tilde{I}_c|^2 + \omega_r T_e \quad (4)$$

In (4), the sign T_e is positive for motoring operation. Active power delivered from the PW and CW sides to the rotor are defined by

$$P_p \triangleq 3\Re\{\tilde{V}_{rp} \tilde{I}_p^*\} = 3\Re\{\tilde{V}_p \tilde{I}_p^*\} - 3R_p |\tilde{I}_p|^2 \quad (5)$$

$$P_c \triangleq 3s_p/s_c \Re\{\tilde{V}_{rc} \tilde{I}_c^*\} = 3\Re\{\tilde{V}_c \tilde{I}_c^*\} - 3R_c |\tilde{I}_c|^2 \quad (6)$$

The electric power converted into mechanical power is obtained from the difference of (3) and (4) as follows:

$$3\Re\{\tilde{V}_c \tilde{I}_c^*\} (1 - s_c/s_p) = 3R_r |\tilde{I}_r|^2 (1 - 1/s_p) + 3R_c |\tilde{I}_c|^2 (1 - s_c/s_p) + \omega_r T_e \quad (7)$$

By substituting (6) into (7), T_e is obtained as follows:

$$T_e = -3\Re\{\tilde{V}_{rc} \tilde{I}_c^*\} / \omega_n + 3R_r |\tilde{I}_r|^2 p_p / \omega_p s_p \quad (8)$$

Based on (8), the torque equation of the BDFIM in the synchronous mode encompasses both synchronous and asynchronous components. However, when considering a BDFIM with 2/4 pole pairs operating at a nominal frequency of 50 Hz, the typical speed range falls within 350 - 650 rpm. In this speed range, the slip of the PW (s_p) is relatively large, rendering the second term in the torque equation negligible. This simplification is employed in [34], where a reduced order model for BDFIMs is developed based on this assumption.

B. Core Model

To simplify the full order model of BDFIMs, it is possible to derive an equivalent circuit for the inner core by excluding the magnetization reactances, the rotor resistance, and the stator resistance. In [32], it is observed that for rotors with different designs, the leakage reactance of the rotor plays a significant role and cannot be neglected. The presence of high spatial harmonic content in the rotor field leads to a substantial leakage inductance. The resulting equivalent circuit (Fig. 5) bears resemblance to a synchronous machine's equivalent circuit, with the exception of neglecting the stator resistance. Consequently, a similar analysis employed for synchronous machines can be applied to study BDFIMs.

The key disparity between the circuits of BDFIMs and synchronous machines lies in the generation of the excitation voltage, denoted as $\tilde{V}_{rc} s_c/s_p$ in BDFIMs. In BDFIMs, the CW induces the voltage through the rotor into the PW. By utilizing the core model, neglecting rotor and stator losses, and neglecting leakage reactances of the stator windings, the power transferred to/from the PW (P_p) can be related to the power transferred to/from the CW (P_c) using the following expression:

$$P_p = 3\Re\{\tilde{V}_{rp} \tilde{I}_{rp}^*\} \quad (9)$$

$$P_c = 3\Re\{\tilde{V}_{rc} \tilde{I}_{rc}^*\} \quad (10)$$

Considering $\tilde{V}_{rc} s_c/s_p = \tilde{V}_{rp} - jX_{lr} \tilde{I}_{rp}$, we have

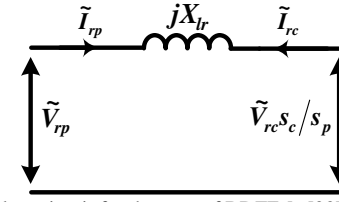


Fig. 5. The equivalent circuit for the core of BDFIMs [32].

$$P_c = -3s_p/s_c \Re\{\tilde{V}_{rp} \tilde{I}_{rp}^* - jX_{lr} \tilde{I}_{rp} \tilde{I}_{rp}^*\} = -3s_p/s_c \Re\{\tilde{V}_{rp} \tilde{I}_{rp}^*\} = -s_p/s_c P_p \quad (11)$$

Using the relationship between the rotor speed, the natural speed, and the slip resulted in (11), Eq. (11) can be rewritten as

$$P_c = (\omega_r/\omega_n - 1)P_p \quad (12)$$

According to (12), a BDFIM can operate either as a motor or a generator. The power flow within the stator windings is contingent upon two factors: 1) the operation mode (motor or generator); and 2) whether the machine is operating at a speed higher or lower than its natural speed.

In the synchronous mode, assuming no power losses, if the rotor speed is below the natural speed, the PW absorbs active power in the motoring mode, while the CW produces active power in the generating mode. If the rotor speed is above the natural speed, the PW and CW absorb active power in the motoring mode, while both windings produce active power in the generating mode. The reactive power flow's direction in the synchronous mode relies on the power factor of stator windings. In the synchronous mode, the voltage variation of the CW yields the same effect as changing the excitation in conventional synchronous machines [33]. In the motoring mode, taking into account power losses, if the rotor speed is below the natural speed, the power produced by the CW is equivalent to the power losses, resulting in zero power flow between the CW and the converter [15].

C. Reduced Order Model

In the synchronous mode, the magnetic fields generated in a BDFIM give rise to three internal machines [34]:

- 1) IM1 with p_p pole pairs created by the PW and the rotor.
- 2) IM2 with p_c pole pairs created by the CW and the rotor.
- 3) DFIM with N_r pole pairs created by the PW and the CW.

Each of the three machines produces its own torque, but the torque components associated with the induction torque of IM1 and IM2 can be neglected for the following reasons:

- The rotor slip caused by the magnetic flux density established in the air gap by the PW and the CW denoted as B_p and B_c , respectively, is significant.
- B_p and B_c rotate in opposite directions relative to the rotor, resulting in torque components that are also in opposite directions. This can be demonstrated by examining the different operating regions of IM1 and IM2, as illustrated in Fig. 6. In each speed range, the active power of the two internal machines always exhibits a opposite sign.

C.1. Steady-state Model

By neglecting the induction torque components, specifically the term R_r/s_p in the steady-state equivalent circuit of BDFIMs, a simplified model can be obtained. As mentioned in Section A, the variation of the PW's slip (s_p) is relatively large

in the rotor speed range. For instance, for a BDFIM with 2/4 pole pair combination, s_p varies between 0.57 and 0.77. Therefore, it is a reasonable approximation to omit the term associated with the induction torque component in (8).

In contrast to conventional IMs, which must have the rotor resistance to produce torque, BDFIMs can achieve the torque production and power conversion without the need for rotor resistance [32]. This is possible because the main torque generation in BDFIMs is attributed to the indirect coupling between the PW and the CW, which is independent of the rotor resistance. By employing the delta-to-star transformation on the rotor loop in Fig. 4 and neglecting the resistance R_r/s_p , the steady state reduced order model of BDFIMs can then be derived, as shown in Fig. 7. In this figure, X_1 , X_2 and X_3 are obtained by

$$X_1 = \frac{X_{pr}X_{lr}}{X_{pr}+X_{cr}+X_{lr}}, X_2 = \frac{X_{cr}X_{lr}}{X_{pr}+X_{cr}+X_{lr}}, X_3 = \frac{X_{pr}X_{cr}}{X_{pr}+X_{cr}+X_{lr}} \quad (13)$$

Ignoring the rotor resistance in the mechanical power equation (7), the terms related to the mechanical power of IMs are omitted. Based on Fig. 7, active power of the PW and the CW can be obtained as follows:

$$P_p = 3\Re\{\tilde{V}_p \tilde{I}_p^*\} = 3\Re\left\{(R_p \tilde{I}_p + j(X_{lp} + X_1) \tilde{I}_p + jX_3(\tilde{I}_p + \tilde{I}_c)) \tilde{I}_p^*\right\} = 3R_p |\tilde{I}_p|^2 + 3\Re\{jX_3 \tilde{I}_p^* \tilde{I}_c\} \quad (14)$$

$$P_c = 3\Re\{\tilde{V}_c \tilde{I}_c^*\} = 3\Re\left\{\left(R_c \frac{s_c}{s_p} \tilde{I}_c + j(X_{lc} + X_2) \tilde{I}_c + jX_3(\tilde{I}_p + \tilde{I}_c)\right) \tilde{I}_c^*\right\} = 3R_c |\tilde{I}_c|^2 + 3s_p/s_c \Re\{jX_3 \tilde{I}_c^* \tilde{I}_p\} \quad (15)$$

By substituting (15) into (7), the torque equation is obtained by

$$T_e = \frac{1}{\omega_r} \left(3\Re\{\tilde{V}_c \tilde{I}_c^*\} \left(1 - \frac{s_c}{s_p}\right) - 3R_c |\tilde{I}_c|^2 \left(1 - \frac{s_c}{s_p}\right) \right) - \frac{1}{\omega_r} \left(\left(3R_c |\tilde{I}_c|^2 + 3s_p/s_c \Re\{jX_3 \tilde{I}_c^* \tilde{I}_p\} \right) \left(1 - s_c/s_p\right) - 3R_c |\tilde{I}_c|^2 \left(1 - s_c/s_p\right) \right) = \frac{3}{\omega_r} (s_p/s_c - 1) \Re\{jX_3 \tilde{I}_c^* \tilde{I}_p\} \quad (16)$$

By knowing

$$s_p/s_c = (\omega_p - N_r \omega_r)/\omega_p \quad (17)$$

For the reduced order model, the torque equation in steady-state can be rewritten as follows:

$$T_e = 3 X_3 / \omega_p N_r \Re\{\tilde{I}_c^* \tilde{I}_p\} \quad (18)$$

C.2. Dynamic Model

In the dynamic mode, flux linkages of the PW, the CW and the rotor are obtained by

$$\vec{\lambda}_p = \left(\frac{L_{lp} + L_{pr}}{L_p} \right) \vec{I}_p + L_{pr} \vec{I}_r \quad (19)$$

$$\vec{\lambda}_c = \left(\frac{L_{lc} + L_{cr}}{L_c} \right) \vec{I}_c + L_{cr} \vec{I}_r \quad (20)$$

$$\vec{\lambda}_r = \left(\frac{L_{lr} + L_{pr} + L_{cr}}{L_r} \right) \vec{I}_r + L_{pr} \vec{I}_p + L_{cr} \vec{I}_c \quad (21)$$

By combining the rotor voltage equation with (19) to (21), the rotor current can be calculated by

$$\vec{I}_r = \frac{-\left(D + j(\omega_a - p_p \omega_r)\right) \left(\frac{L_{pr}}{L_p} \vec{\lambda}_p + \frac{L_{cr}}{L_c} \vec{\lambda}_c \right)}{R_r + \left(D + j(\omega_a - p_p \omega_r)\right) \left(L_r - \frac{L_{pr}^2}{L_p} - \frac{L_{cr}^2}{L_c} \right)} \quad (22)$$

For the nested loop rotors, the rotor resistance, which is the first term in the denominator of (22), is generally lower than the second term, so it can be omitted [55]. By substituting (19) and (20) into (22), we have

$$\vec{I}_r = -(L_{pr}/L_r) \vec{I}_p - (L_{cr}/L_r) \vec{I}_c \quad (23)$$

Now, substituting (23) into (19) and (20), we have

$$\vec{\lambda}_p = \left(\frac{L_{lp} + L_1 + L_3}{L_{op}} \right) \vec{I}_p + (-L_3) \vec{I}_c \quad (24)$$

$$\vec{\lambda}_c = (-L_3) \vec{I}_p + \left(\frac{L_{lc} + L_2 + L_3}{L_{oc}} \right) \vec{I}_c \quad (25)$$

Therefore, in the dynamic reduced order model, PW and CW flux linkages are obtained in (24) and (25). In the dynamic full order model, the electromagnetic torque can be calculated by

$$T_e = \frac{3}{2} p_p \text{Im}\{\vec{\lambda}_p^* \vec{I}_p\} + \frac{3}{2} p_c \text{Im}\{\vec{\lambda}_c^* \vec{I}_c\} \quad (26)$$

If the PW and CW currents from (19) and (20) are substituted into (26), the electromagnetic torque can be decomposed into three components as follows:

$$T_e = T_{IM1} + T_{IM2} + T_{DFIM} = 1.5 \frac{L_{pr}}{L_p L_r \sigma} p_p \text{Im}\{\vec{\lambda}_p \vec{\lambda}_r^*\} + 1.5 \frac{L_{cr}}{L_c L_r \sigma} p_c \text{Im}\{\vec{\lambda}_r \vec{\lambda}_c^*\} + 1.5 \frac{L_3}{L_p L_c \sigma} N_r \text{Im}\{\vec{\lambda}_p \vec{\lambda}_c^*\} \quad (27)$$

where $\sigma = L_{pr}^2/L_p L_r + L_{cr}^2/L_c L_r - 1$, and $L_3 = L_{pr} L_{cr}/L_r$.

In the reduced order model, the first two terms of (27), which correspond to the induction torques, are neglected. This implies that the rotor flux linkage is assumed to be zero. Ref. [34] shows that based on simulations and experimental results, neglecting T_{IM1} and T_{IM2} will not cause a substantial error in calculations.

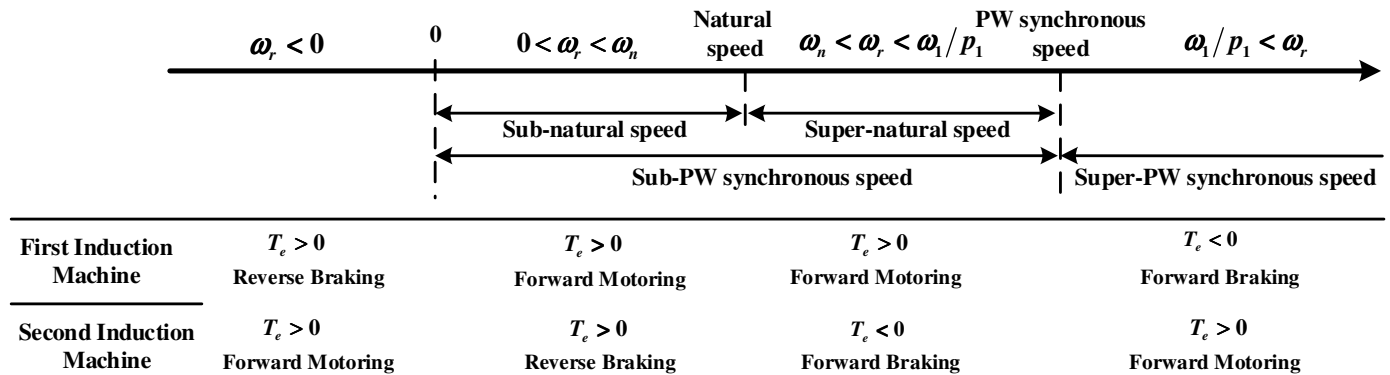


Fig. 6. Operating regions of two IMs inside a BDFIM.

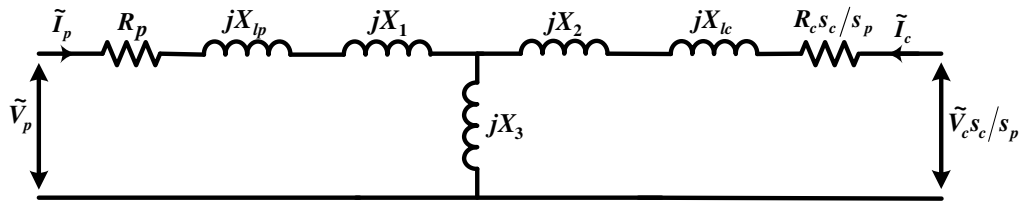


Fig. 7. The steady state reduced order model for BDFIMs in the synchronous mode [34].

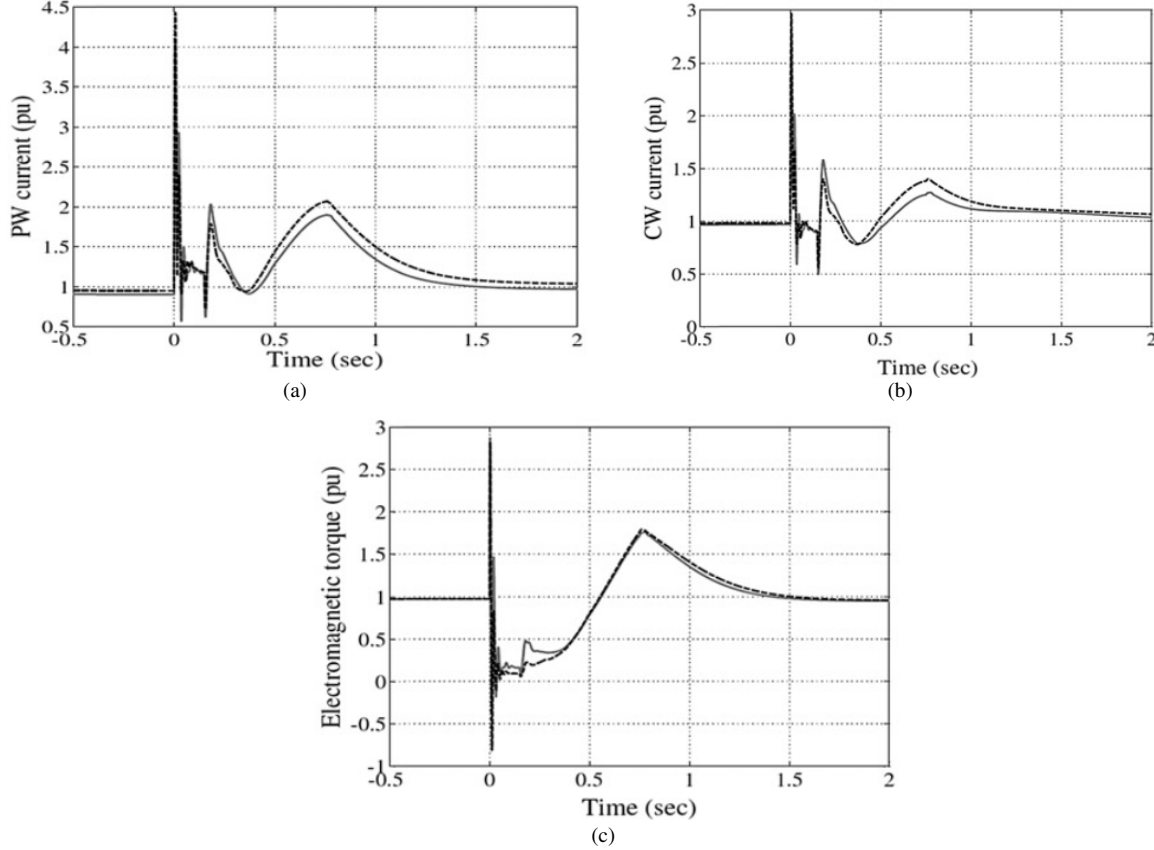


Fig. 8. Simulation results of complete and simplified dynamic models of BDFIMs (solid line for the full order model, dashed line for the reduced order model): (a) PW current, (b) CW current, (c) Electromagnetic torque [34].

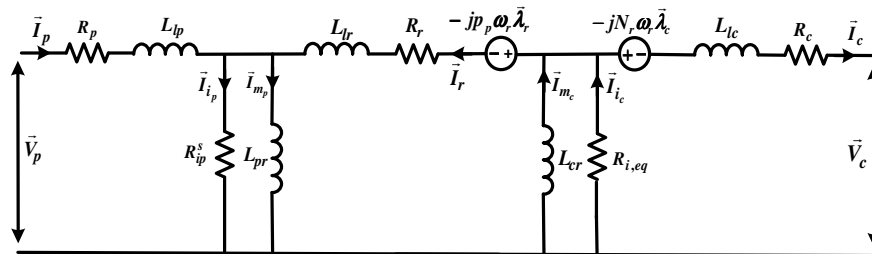


Fig. 9. Space vector equivalent circuit of BDFIMs including iron losses in a stationary reference frame (a full order model) [48].

As a result of this simplification, the torque equation can be expressed by

$$T_e \approx 1.5 \frac{L_3}{L_p L_c \sigma} N_r \Im \{ \tilde{\lambda}_p \tilde{\lambda}_c^* \} \quad (28)$$

To evaluate the performance of the simplified model during transient scenarios, a time-domain simulation is conducted on a BDFIM in [34]. The simulation assumes a constant and normalized input mechanical power of 1 per unit. Subsequently, a sudden 85% voltage dip is applied to all three phases at the machine terminal. Fig. 8 shows a good agreement between the reduced order model and the full order model.

D. Reduced Order Dynamic Model including Iron Losses

To derive the full order dynamic model considering iron losses, the space vector equations in a stationary reference frame, neglecting iron losses, can be expressed by

$$\tilde{V}_p^s = R_p \tilde{I}_p^s + d\tilde{\lambda}_p^s / dt \quad (29)$$

$$\tilde{V}_c^s = R_c \tilde{I}_c^s + d\tilde{\lambda}_c^s / dt - jN_r \omega_r \tilde{\lambda}_c^s \quad (30)$$

$$\tilde{V}_r^s = 0 = R_r \tilde{I}_r^s + d\tilde{\lambda}_r^s / dt - jp_p \omega_r \tilde{\lambda}_r^s \quad (31)$$

The iron loss resistances on the PW and CW sides (R_{ip}^s and $R_{i,eq}$) [48] are included in parallel with the magnetizing

inductances L_{pr} and L_{cr} , respectively, following a conventional method to model iron losses in IMs [56]. This results in a full order model in a stationary reference frame, as shown in Fig. 9.

Equation (32) is a general relation for the transfer from one reference frame to another arbitrary reference frame.

$$\vec{x}_2 = \vec{x}_1 e^{-j\theta_c} \quad (32)$$

The space vectors in the current and new reference frames are denoted by \vec{x}_1 and \vec{x}_2 , respectively. The angle θ_c represents the phase difference between the two reference frames ($\theta_2 - \theta_1$). To transfer a stationary reference frame to an arbitrary reference frame with the angular velocity ω_a , the transformation $\vec{x}_2 = \vec{x}_1 e^{j\theta_a}$ is utilized. By applying this transformation, the voltage and the flux linkage equations for the PW, the CW, and the rotor can be derived as follows:

$$\vec{V}_p = R_p \vec{I}_p + d\vec{\lambda}_p/dt + j\omega_a \vec{\lambda}_p \quad (33)$$

$$\vec{V}_c = R_c \vec{I}_c + d\vec{\lambda}_c/dt + j(\omega_a - N_r \omega_r) \vec{\lambda}_c \quad (34)$$

$$\vec{V}_r = 0 = R_r \vec{I}_r + d\vec{\lambda}_r/dt + j(\omega_a - p_p \omega_r) \vec{\lambda}_r \quad (35)$$

$$\vec{\lambda}_p = L_{lp} \vec{I}_p + L_{pr} \vec{I}_{mp} \quad (36)$$

$$\vec{\lambda}_c = L_{lc} \vec{I}_c + L_{cr} \vec{I}_{mc} \quad (37)$$

$$\vec{\lambda}_r = L_{lr} \vec{I}_r + L_{pr} \vec{I}_{mp} + L_{cr} \vec{I}_{mc} \quad (38)$$

From (33) to (38), the dynamic equivalent circuit of BDFIMs is obtained considering iron losses in an arbitrary reference frame, as shown in Fig. 10. The torque equation for the full order model is derived based on the input active power equation. The active power comprises the power stored in the magnetic field of the machine, the power converted into mechanical power, and power losses. During steady-state operations, the power stored in the magnetic field remains constant since the flux density in the air gap has a constant amplitude. Therefore, after the initial transient, no energy is being stored in the field. The torque equation for the machine with iron losses is derived by

$$T_e = \frac{3}{2} p_p L_{pr} \text{Im} \{ \vec{I}_{mp} \vec{I}_r^* \} - \frac{3}{2} p_c L_{cr} \text{Im} \{ \vec{I}_{mc} \vec{I}_r^* \} \quad (39)$$

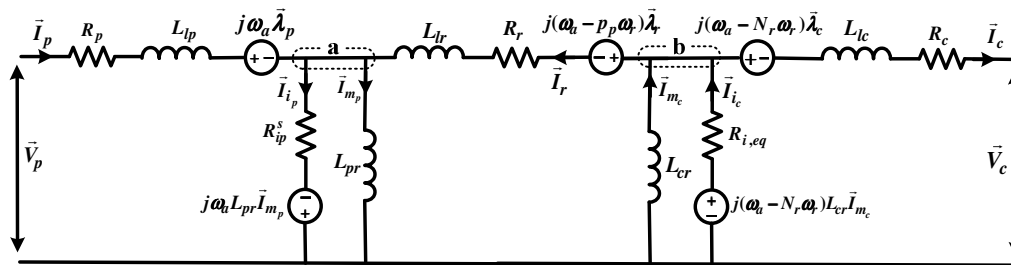


Fig. 10. The space vector equivalent circuit of BDFIMs including iron losses (a full order model) [48].

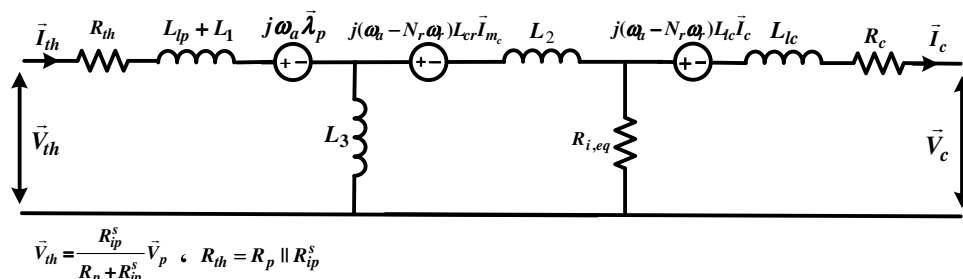


Fig. 11. The reduced order dynamic equivalent circuit of BDFIMs [48].

The process used to derive the full order model can also be applied to derive the reduced order model. By neglecting the rotor resistance in the full order equivalent circuit, we obtain the reduced order model, as shown in Fig. 11. L_1 , L_2 and L_3 are obtained based on inductances of the full order model by

$$L_1 = \frac{L_{pr} L_{lr}}{L_{pr} + L_{cr} + L_{lr}}, \quad L_2 = \frac{L_{cr} L_{lr}}{L_{pr} + L_{cr} + L_{lr}}, \quad L_3 = \frac{L_{pr} L_{cr}}{L_{pr} + L_{cr} + L_{lr}} \quad (40)$$

Ref. [48] investigates dynamic behaviors of a full order model and a reduced order model during a three-phase fault. The fault occurs at $t = 2$ s, and is cleared after two seconds. With the BDFIM's stator current equal to zero, the electromagnetic torque is also zero, so the load torque decelerates the BDFIM's rotor speed. The acceptable accuracy of the reduced order model during the three-phase fault is shown in Fig. 12.

E. Dynamic full-order model including iron losses and magnetic saturation effects

To derive the full nonlinear model of BDFIMs in an arbitrary reference frame, voltage space vector equations for the PW, the CW, and the rotor are expressed by (33)-(35). By incorporating the saturation effect into these equations, the first-time derivatives of the d- and q-axis components of the PW magnetizing flux in an arbitrary reference frame are derived by

$$d\lambda_{mpd}/dt = L_{mp} di_{mpd}/dt + i_{mpd} dL_{mp}/dt \quad (41)$$

$$d\lambda_{mpq}/dt = L_{mp} di_{mpq}/dt + i_{mpq} dL_{mp}/dt \quad (42)$$

Under saturated conditions, the first-time derivative of the magnetizing inductance is computed as follows:

$$dL_{mp}/dt = ((L_p - L_{mp})/|i_{mp}|) d|i_{mp}|/dt \quad (43)$$

where L_p and L_{mp} are dynamic and static time variant inductances of the PW, respectively. L_{mp} represents the chord slope of the PW magnetizing curve, while L_p refers to the tangent slope. Unlike the linear magnetic condition where the tangent-slope inductance is equal to the chord-slope inductance,

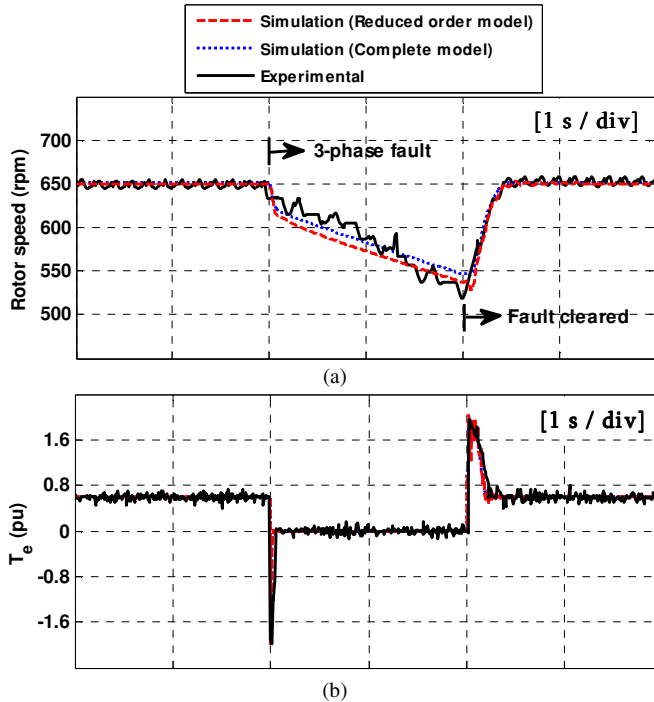


Fig. 12. Dynamic performance of a reduced order model including iron losses during a three-phase fault; (a) rotor speed, (b) electromagnetic torque [48].

under saturated conditions, the tangent-slope inductance is non-zero. So, these inductances are defined by

$$L_p = d|\vec{\lambda}_{mp}|/d|i_{mp}|, \quad L_{mp} = |\vec{\lambda}_{mp}|/|i_{mp}| \quad (44)$$

The magnetizing flux linkages are calculated using the conventional no-load test procedure. In (43), the first-time derivative of the amplitude of magnetizing current ($|\vec{i}_{mp}|$) can be determined by

$$d|\vec{i}_{mp}|/dt = \cos \mu_p di_{mpd}/dt + \sin \mu_p di_{mpq}/dt \quad (45)$$

where μ_p is the angular displacement of \vec{i}_{mp} with respect to the direct axis of an arbitrary reference frame. By substituting (43)

into (41) and (42), the first-time derivative of the d - and q -axis components of the PW magnetizing flux can be rewritten by

$$d\lambda_{mpd}/dt = L_{Mpd} di_{mpd}/dt + L_{pdq} di_{mpq}/dt \quad (46)$$

$$d\lambda_{mpq}/dt = L_{Mpq} di_{mpq}/dt + L_{pdq} di_{mpd}/dt \quad (47)$$

By obtaining the CW magnetizing curve, as well as dynamic and static inductances, the first-time derivatives of the d - and q -axis components of the CW and rotor magnetizing fluxes can be determined similarly by considering the saturation effect:

$$d\lambda_{mcd}/dt = L_{Mcd} di_{mcd}/dt + L_{cdq} di_{mcq}/dt \quad (48)$$

$$d\lambda_{mcq}/dt = L_{Mcq} di_{mcq}/dt + L_{cdq} di_{mcd}/dt \quad (49)$$

$$d\lambda_{rd}/dt = L_{lr} di_{rd}/dt + L_{Mpd} di_{mpd}/dt + L_{pdq} di_{mpq}/dt + L_{Mcd} di_{mcd}/dt + L_{cdq} di_{mcq}/dt \quad (50)$$

$$d\lambda_{rq}/dt = L_{lr} di_{rq}/dt + L_{Mpq} di_{mpq}/dt + L_{pdq} di_{mpd}/dt + L_{Mcq} di_{mcq}/dt + L_{cdq} di_{mcd}/dt \quad (51)$$

where $L_{Mpd,q}$, $L_{Mcd,q}$, and $L_{p,cdq}$ depend on both static and dynamic inductances [49]. Under linear magnetic conditions, the static inductances are equal to the dynamic inductances, so $L_{Mpd} = L_{Mpq} = L_{mp}$, $L_{Mcd} = L_{Mcq} = L_{mc}$, and $L_{pdq} = L_{cdq} = 0$.

The saturated d - q full model of BDFIMs in an arbitrary reference frame, considering iron losses, can be finally derived. In this model (Fig. 13), the orthogonal d - q axes are coupled through the cross-coupling inductances, L_{pdq} and L_{cdq} .

To evaluate this model's dynamic performance, a three-phase terminal fault is applied to a 50 Hz power system under the steady state by setting the source voltage to zero at $t = 0.5$ s. The load torque is adjusted to 50% of the rated torque, and the machine operates in the synchronous mode. Due to this fault, the terminal voltage of the machine abruptly decreases to zero, causing the transient fluctuations in both PW and CW currents. However, the fluctuations are gradually dampened before the fault is cleared, and eventually, the machine's currents settle back to zero. After a duration of 25 cycles, the fault is cleared, and the source voltage is restored, and the machine returns to its initial operation state. Simulation results in Fig. 14 closely match experimental results. The discrepancies between theoretical and experimental tests can be attributed to

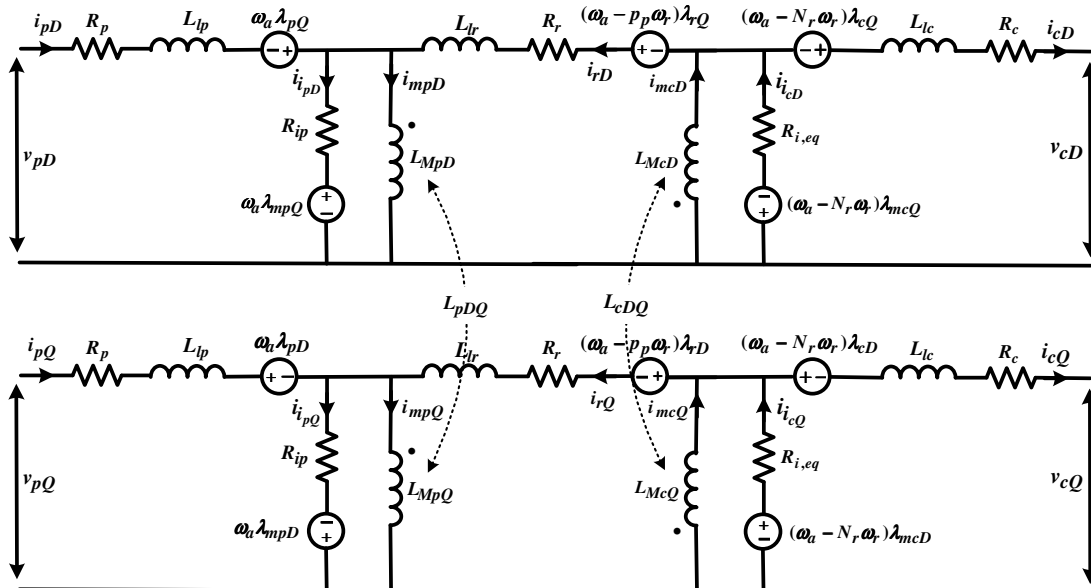


Fig. 13. The saturated two-axis (d - q) full model of BDFIMs including the iron losses effect in an arbitrary reference frame [49].

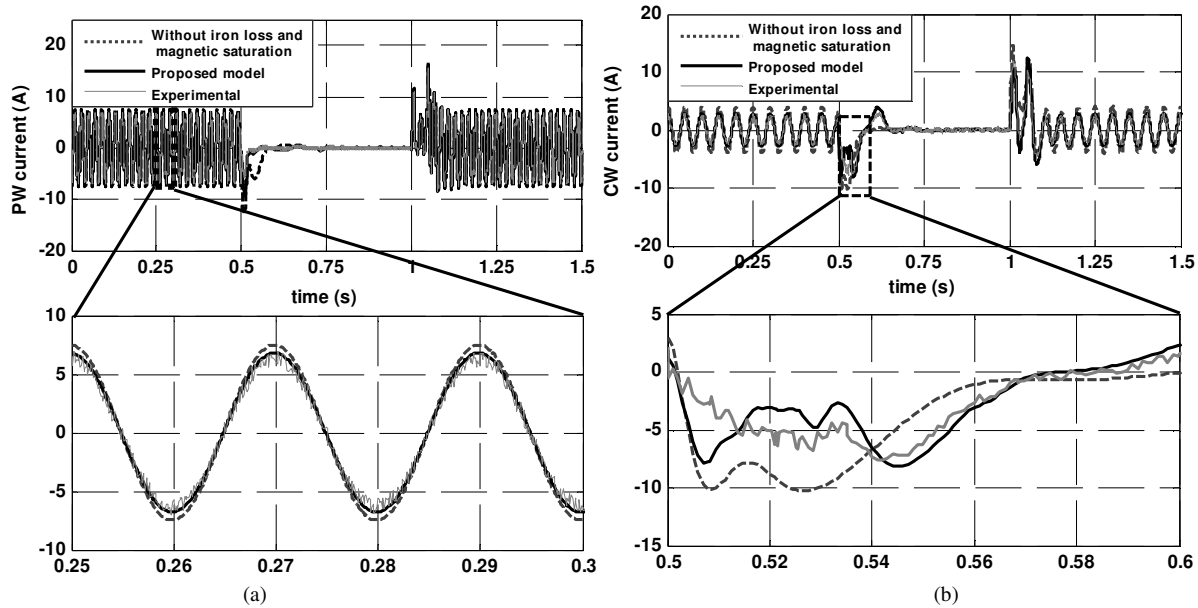


Fig. 14. Currents of the PW and CW during a terminal fault (Phase A); (a) PW current, (b) CW current. ($f_{PW} = 50 \text{ Hz}$, $f_{CW} = 20 \text{ Hz}$) [49].

TABLE I
COMPARISON OF EXISTING BDFIM MODELS IN THE LITERATURE

Ref.	Rotor resistance considered?	Iron losses considered?	Magnetic saturation considered?	Dynamic or steady-state modelling?
[6]	Yes	No	No	Dynamic
[29]	Yes	No	No	Dynamic
[32]	No	No	No	Steady-state
[33]	Yes	No	No	Steady-state
[34]	No	No	No	Dynamic/Steady-state
[46]	Yes	Yes	No	Steady-state
[47]	Yes	Yes	No	Steady-state
[48]	Yes	Yes	No	Dynamic
[49]	No	Yes	No	Dynamic
[50]	Yes	Yes	Yes	Dynamic

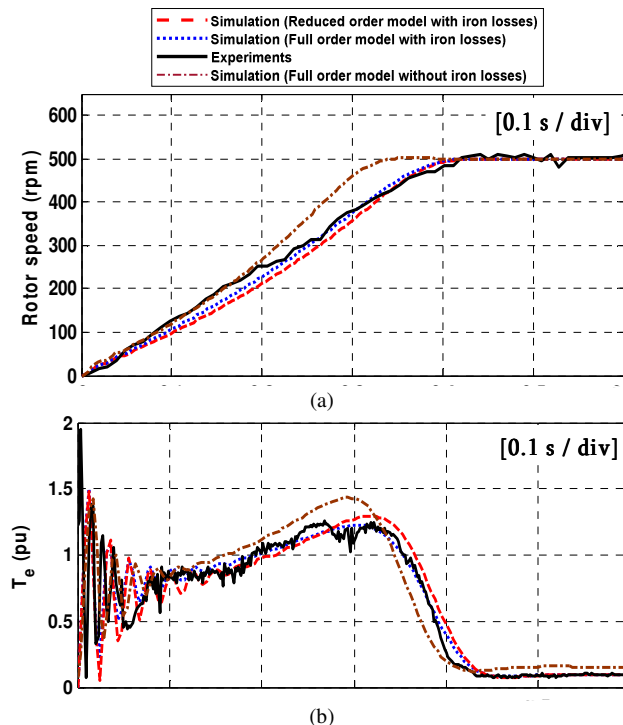


Fig. 15. The performance of BDFIM during free acceleration; (a) Rotor speed, (b) Electromagnetic torque.

factors, such as stray load losses and mechanical losses, not being considered in the modeling approach.

It is valuable to provide a comparison of existing BDFIM models in the literature. Accordingly, key attributes of ten existing BDFIM models have been summarized in Table I. Each model serves a specific purpose based on a desired level of accuracy.

We have conducted a comparative study using three BDFIM electrical equivalent circuits proposed in the literature, as shown in Fig. 15 through simulations and experiments: 1) a full order model excluding iron losses in [33], 2) a full order model including iron losses in [48], and 3) a reduced order model including iron losses in [49]. In this study, the BDFIM is started in a cascade induction mode by shorting the CW and turning on the three low-side (or high-side) inverter switches. When the rotor speed reaches the natural synchronous speed, IGBTs are controlled in a normal way to lock into the synchronous mode. In Fig. 15, the rotor speed accelerates to the natural synchronous speed; the settling time increases and the acceleration decreases when iron losses are taken into account. The electromagnetic torque curves in Fig. 15 indicate that the torque decreases when considering iron losses.

IV. FUTURE RESEARCH DIRECTIONS

The future research directions are recommended as follows:

A reduced order full-saturated model: Deriving a dynamic model by taking into account the effect of magnetic saturation and iron losses can be very useful to study the BDFIM's behaviors. In electrical machines modeling, two approaches are generally used to consider the magnetic saturation effect. In the first approach, a variable inductance as a nonlinear function of the magnetizing current is used rather than a constant magnetizing inductance [57]. The second approach utilizes a complete nonlinear model that takes into account time variations of the magnetizing inductance, which results in different voltage equations compared to the unsaturated model. To represent this change, a new term called "dynamic cross-saturation effects" is incorporated into the full nonlinear model, which is neglected in the simplified model [58], [59]. The full nonlinear model offers superior accuracy [60] and faster responses [61] compared to the simplified model. Although a complete saturated model, accounting for the iron losses effect, has been proposed for BDFIMs in [49], it is relatively complex and hard to be used to develop model-based control strategies. Therefore, a reduced order model with high accuracy is needed. This model can facilitate the performance analysis of BDFIMs and various advanced control techniques development, such as the optimized-efficiency strategy.

Multi-physics modeling: The BDFIM involves multiple physical phenomena, such as electrical, magnetic, thermal, and mechanical aspects. Integrating these different physics into a comprehensive electrical equivalent circuit model can represent more realistic behaviors of the machine. Researchers can explore methodologies to develop multi-physics equivalent circuit models for BDFIMs.

High-frequency effects: Traditional electrical equivalent circuits are designed for low and medium-frequency applications. However, with the increasing demand for high-frequency electric machines, there is a need for equivalent circuit models that can accurately represent high-frequency behaviors. Developing high-frequency equivalent circuit models and associated parameter extraction techniques can be considered for BDFIMs electrical modeling.

Integration of advanced materials: Emerging materials, such as advanced magnetic materials and superconductors, have unique electrical and magnetic properties that may require novel equivalent circuit models. Future research can focus on developing equivalent circuit models that can accurately represent behaviors of BDFIMs with advanced materials.

Real-time simulation and hardware-in-the-loop: Real-time simulation and hardware-in-the-loop techniques are valuable tools for testing and validating electrical machine's control strategies. Future research can explore methodologies to integrate electrical equivalent circuits of BDFIMs into real-time

simulation platforms and hardware-in-the-loop setups, enabling rapid prototyping and performance evaluation of BDFIMs.

V. CONCLUSION

Electrical equivalent circuit models are essential to analyze behaviors of BDFIMs and develop advanced control strategies. In this paper, various electrical equivalent circuit models for BDFIMs are reviewed, from the full order model to the reduced order model, by considering influencing factors, such as iron losses, the magnetic saturation, and the rotor resistance. The full order model serves as a comprehensive representation of a BDFIM's electrical characteristics but is complex; by simplifying this full order model and neglecting certain components, such as the induction torque and rotor resistance, we can obtain the reduced order model that is less complex with fewer electrical state variables and provides practical approximations of the full order model. By incorporating equivalent resistances for iron losses, the influence of iron losses on the machine's performance, particularly under dynamic conditions, can be accurately represented. Two common approaches are also highlighted to address the effect of magnetic saturation in the models. Further research could focus on refining the models to incorporate additional factors and improve their accuracy for specific applications of BDFIMs.

REFERENCES

- [1] T. D. Strous, H. Polinder, and J. A. Ferreira, "Brushless doubly-fed induction machines for wind turbines: developments and research challenges," *IET Electric Power Applications*, vol. 11, no. 6, pp. 991-1000, July 2017.
- [2] G. H. Rawcliffe, "Improvements in or Relating to Rotary Electric Machines", UK Patent 974082A, Feb. 26, 1960.
- [3] A. Broadway, and L. Burbridge, "Self-Cascaded Machine: A Low-Speed Motor or High-Frequency Brushless Alternator", *Proceedings, Institution of Electrical Engineers*, vol. 117, no. 7, pp. 1277-1290, July 1970.
- [4] P. Rochelle, R. Spee and A. K. Wallace, "The effect of stator winding configuration on the performance of brushless doubly-fed machines in adjustable speed drives," *Conference Record of the 1990 IEEE Industry Applications Society Annual Meeting*, Seattle, WA, USA, pp. 331-337, 1990.
- [5] R. Li, A. Wallace, and R. Spee, "Dynamic Simulation of Brushless Doubly-Fed Machines," *IEEE Transactions on Energy Conversion*, vol. 6, no. 3, pp. 445-452, Sep. 1991.
- [6] R. Li, A. Wallace, R. Spee, and Y. Wang, "Two-Axis Model Development of Cage-Rotor Brushless Doubly-Fed Machines," *IEEE Transactions on Energy Conversion*, vol. 6, no. 3, pp. 453-460, Sep. 1991.
- [7] R. Li, R. Spee, A. Wallace, and G. Alexander, "Synchronous Drive Performance of Brushless Doubly-Fed Motors", *IEEE Transactions on Industry Applications*, vol. 30, no. 4, pp. 963-970, Aug. 1994.
- [8] R. Li, A. Wallace, and R. Spee, "Determination of Converter Control Algorithms for Brushless Doubly-Fed Induction Motor Drives Using Floquet and Lyapunov Techniques," *IEEE Transactions on Power Electronics*, vol. 10, no. 1, pp. 78-85, Jan. 1995.
- [9] A. Wallace, P. Rochelle, and R. Spee, "Rotor Modeling and Development for Brushless Doubly-Fed Machines," *Electric Machines and Power Systems*, vol. 23, no. 6, pp. 703-715, Feb. 1994.
- [10] S. Abdi, E. Abdi, R. McMahon "Experimental and Finite Element Studies of a 250kW Brushless Doubly Fed Induction Generator" *IET Journal of Engineering*, vol. 2019, no. 12, pp. 8489-8495, Feb. 2019.
- [11] S. Abdi, E. Abdi, A. Oraee, R. McMahon, "Optimisation of Magnetic Circuit for Brushless Doubly Fed Machines", *IEEE Transactions on Energy Conversion*, vol. 30, no. 3, pp. 1611-1620, Dec. 2015.
- [12] A. Oraee, E. Abdi, S. Abdi, R. McMahon, P. Tavner, "Effects of Rotor Winding Structure on the BDFM Equivalent Circuit Parameters", *IEEE Transactions on Energy Conversion*, vol. 30, no. 4, Dec. 2015.
- [13] S. Abdi, E. Abdi, A. Oraee, R. McMahon, "Equivalent Circuit Parameters for Large Brushless Doubly Fed Machines (BDFM)", *IEEE Transactions on Energy Conversion*, vol. 29, no. 3, pp. 706-716, Sep. 2014.

- [14] A. K. Wallace, R. Spee and H. K. Lauw, "The potential of brushless doubly-fed machines for adjustable speed drives," *Annual Technical Conference on Pulp and Paper Industry*, Seattle, USA, pp. 45-50, 1990.
- [15] E. Abdi, R. McMahon, P. Malliband, S. Shao, M. E. Mathekg, P. Tavner, S. Abdi, A. Oraee, and T. Long "Performance Analysis and Testing of a 250 kW Medium-Speed Brushless Doubly-Fed Induction Generator," *IET Renewable Power Generation*, vol. 7, no. 6, pp. 631-638, Nov. 2013.
- [16] H. R. Mosaddegh and H. Abootorabi Zarchi, "Maximum Torque per Ampere Control of Brushless Doubly Fed Induction Machine using Variable Structure Approach," *2014 22nd Iranian Conference on Electrical Engineering (ICEE)*, Tehran, Iran, pp. 677-682, 2014.
- [17] H. R. Mosaddegh and H. Abootorabi Zarchi, "Variable Structure Direct Torque Control of Brushless Doubly Fed Induction Generator for Wind Turbine Applications," *22nd Iranian Conference on Electrical Engineering (ICEE)*, Tehran, Iran, pp. 671-676, 2014.
- [18] H. Mosaddegh Hesar, and H. Abootorabi Zarchi, "Maximum Torque per Ampere Control of Brushless Doubly Fed Induction Generator Using Variable Structure Approach for Wind Turbine Applications," *Journal of Electrical Systems and Signals*, vol. 3, no. 1, pp. 1-8, May 2015.
- [19] H. Mosaddegh Hesar, X. Liang, M. A. Salahmanesh, M. A. Khoshhava and S. Abdi, "Vector Control of Brushless Doubly-Fed Induction Machines Based on Highly Efficient Nonlinear Controllers," *IEEE Transactions on Industrial Electronics*, vol. 71, no. 6, pp. 5641-5652, June 2024
- [20] H. Mosaddegh Hesar, H. Abootorabi Zarchi, G. Arab Markadeh and A. Khazae, "Maximum Torque Per Total Ampere Strategy for Vector-Controlled Brushless Doubly Fed Induction Machine Drive Taking Iron Loss into Account," *IEEE Transactions on Power Electronics*, vol. 37, no. 11, pp. 13598-13605, Nov. 2022.
- [21] H. Mosaddegh Hesar, H. Abootorabi Zarchi and G. Arab Markadeh, "Online MTPA and MTPA Control of Brushless Doubly Fed Induction Motor Drives," *IEEE Transactions on Power Electronics*, vol. 36, no. 1, pp. 691-701, Jan. 2021.
- [22] H. Mosaddegh, H. Abootorabi Zarchi and G. Arab Markadeh, "Stator Flux Oriented Control of Brushless Doubly Fed Induction Motor Drives Based on Maximum Torque per Total Ampere Strategy," *10th International Power Electronics, Drive Systems and Technologies Conference (PEDSTC)*, Shiraz, Iran, pp. 84-89, 2019.
- [23] N. Patin, E. Monmasson and J. P. Louis, "Analysis and control of a cascaded doubly-fed induction generator," *31st Annual Conference of IEEE Industrial Electronics Society (IECON 2005)*, Raleigh, NC, USA, 2005.
- [24] Y. Liu, W. Xu, J. Zhu, and F. Blaabjerg, "Sensorless Control of Standalone Brushless Doubly Fed Induction Generator Feeding Unbalanced Loads in a Ship Shaft Power Generation System," *IEEE Transactions on Industrial Electronics*, vol. 66, no. 1, pp. 739-749, Jan. 2019.
- [25] R. Sadeghi, S. M. Madani, M. R. Agha-kashkooli, and M. Ataei, "Reduced Order Model of Cascaded Doubly Fed Induction Generator for Aircraft Starter/Generator," *IET Electric Power Applications*, vol. 12, no. 6, pp. 757-766, Jan. 2018.
- [26] P. Löhdefink, A. Dietz and A. Möckel, "Direct Drive Concept for Heavy-Duty Traction Applications with the Brushless Doubly-Fed Induction Machine," *Thirteenth International Conference on Ecological Vehicles and Renewable Energies (EVER)*, Monte Carlo, Monaco, 2018, pp. 1-6.
- [27] M. Cheng and P. Han, "A dual-stator brushless doubly-fed induction motor for EV/HEV applications," 2014 International Conference on Intelligent Green Building and Smart Grid (IGBSG), Taipei, Taiwan, 2014, pp. 1-6, doi: 10.1109/IGBSG.2014.6835258.
- [28] R. Spee, A. K. Wallace, and H. K. Lauw, "Performance Simulation of Brushless Doubly-Fed Adjustable Speed Drives," *Conference Record of the IEEE Industry Applications Society Annual Meeting*, San Diego, USA, Oct. 1989.
- [29] A. K. Wallace, R. Spée, and H. K. Lauw, "Dynamic Modelling of Brushless Doubly-Fed Machines," *Conference Record of the IEEE Industry Applications Society Annual Meeting*, San Diego, USA, Oct. 1989.
- [30] P. Roberts, "A Study of Brushless Doubly-Fed (Induction) Machines," Ph.D. diss., Univ. Cambridge, Cambridge, UK, Sep. 2004.
- [31] M. S. Boger, A. K. Wallace, R. Spee, and Ruqi Li, "General Pole Number Model of the Brushless Doubly-Fed Machine," *IEEE Transactions Industry Applications*, vol. 31, no. 5, pp. 1022-1028, Sep. 1995.
- [32] R. A. McMahon, P. C. Roberts, X. Wang, and P. J. Tavner, "Performance of BDFM as Generator and Motor," *IEE Electric Power Applications*, vol. 153, no. 2, pp. 289-299, Mar. 2006.
- [33] P. C. Roberts, R. A. McMahon, P. J. Tavner, J. M. Maciejowski and T. J. Flack, "Equivalent Circuit for the Brushless Doubly-Fed Machine (BDFM) including Parameter Estimation and Experimental Verification," *IEE Electric Power Applications*, vol. 152, no. 4, pp. 933-942, July 2005.
- [34] S. Tohidi, "Analysis and Simplified Modelling of Brushless Doubly Fed Induction Machine in Synchronous Mode of Operation," *IET Electric Power Applications*, vol. 10, no. 2, pp. 110-116, Feb. 2016.
- [35] A. T. de Almeida, F. J. T. E. Ferreira and G. Baoming, "Beyond Induction Motors - Technology Trends to Move Up Efficiency," *IEEE Transactions on Industry Applications*, vol. 50, no. 3, pp. 2103-2114, May-June 2014.
- [36] E. Levi, "Impact of Iron Loss on Behavior of Vector Controlled Induction Machines," *IEEE Transactions Industry Applications*, vol. 31, no. 6, pp. 1287-1296, Dec. 1995.
- [37] H. Gorginpour, H. Oraee and E. Abdi, "Calculation of Core and Stray Load Losses in Brushless Doubly Fed Induction Generators," *IEEE Transactions on Industrial Electronics*, vol. 61, no. 7, pp. 3167-3177, July 2014.
- [38] M. N. Hashemnia, F. Tahami and E. Oyarbide, "Investigation of Core Loss Effect on Steady-State Characteristics of Inverter Fed Brushless Doubly Fed Machines," *IEEE Transactions on Energy Conversion*, vol. 29, no. 1, pp. 57-64, March 2014.
- [39] A. C. Ferreira, and S. Williamson, "Time-Stepping Finite-Element Analysis of Brushless Doubly-Fed Machine Taking Iron Loss and Saturation into Account," *IEEE Transactions on Industry Applications*, vol. 35, no. 3, pp. 583-588, May-June 1999.
- [40] H. Gorginpour, H. Oraee and R. A. McMahon, "A Novel Modeling Approach for Design Studies of Brushless Doubly-Fed Induction Generator Based on Magnetic Equivalent Circuit," *IEEE Transactions on Energy Conversion*, vol. 28, no. 4, pp. 902-912, Dec. 2013.
- [41] S. Abdi, E. Abdi, H. Toshani, R. McMahon, "A new iron loss model for brushless doubly fed machines with hysteresis and field rotational losses", *IEEE Transactions on Energy Conversion*, vol.36, pp. 3221 - 3230, 2021.
- [42] S. Abdi, E. Abdi, R. McMahon, "Rotational Iron Losses in Brushless Doubly Fed Machines", *IEEE International Conference on Electrical Machines (ICEM)*, Valencia, Spain, September 2022.
- [43] Ahmadian, M., B. Jandaghi, and H. Oraee, "Hysteresis Loss in Brushless Doubly Fed Induction Machines," *International Conference on Renewable Energy and Power Quality*, vol.1, no.9, pp. 975-980, May 2011.
- [44] A. Ramchandran, "Frequency-Domain, Parameter Estimation for the Brushless Doubly-Fed Machine," PhD diss., Oregon State Univ., 1995.
- [45] M. N. Hashemnia, F. Tahami, P. Tavner, and S. Tohidi, "Steady State Analysis and Performance of a Brushless Doubly Fed Machine accounting for Core Loss," *IET Electric Power Applications*, vol. 7, no. 3, pp. 170-178, Mar. 2013.
- [46] M. Yousefian, H. A. Zarchi, and H. Gorginpour, "Modified Steady State Modelling of Brushless Doubly Fed Induction Generator Taking Core Loss Components into Account," *IET Electric Power Applications*, vol. 13, no. 9, pp. 1402-1412, Sep. 2019.
- [47] M. N. Hashemnia, and F. Tahami, "Dynamic Modeling and Simulation of Brushless Doubly Fed Induction Machine in Consideration of Core Loss," *38th Annual Conference on IEEE Industrial Electronics Society*, Montreal, Canada, Oct. 2012.
- [48] H. Mosaddegh Hesar, H. Abootorabi Zarchi and G. A. Markadeh, "Modeling and Dynamic Performance Analysis of Brushless Doubly Fed Induction Machine Considering Iron Loss," *IEEE Transactions on Energy Conversion*, vol. 35, no. 1, pp. 193-202, March 2020.
- [49] H. Mosaddegh Hesar, M. A. Salahmanesh and H. Abootorabi Zarchi, "Generalized Analysis of Brushless Doubly Fed Induction Machine Taking Magnetic Saturation and Iron Loss into Account," *IEEE Transactions on Industrial Electronics*, vol. 68, no. 8, pp. 6470-6480, Aug. 2021.
- [50] S. Williamson, A. C. Ferreira, and A. Wallace, "Generalized Theory of the Brushless Doubly-Fed Machine-Part I: Analysis," *IEE Electric Power Applications*, vol. 144, no. 2, pp. 111-122, Mar. 1997.
- [51] R. Li, R. Spee, A. Wallace, and G. Alexander, "Synchronous Drive Performance of Brushless Doubly-Fed Motors", *IEEE Transactions Industry Applications*, vol. 30, no. 4, pp. 963-970, Aug. 1994.
- [52] S. Abdi, E. Abdi and R. McMahon, "A Study of Unbalanced Magnetic Pull in Brushless Doubly Fed Machines," *IEEE Transactions on Energy Conversion*, vol. 30, no. 3, pp. 1218-1227, Sept. 2015.
- [53] S. Abdi, A. Grace, E. Abdi and R. McMahon, "A new optimized rotor design for brushless doubly fed machines," 20th International Conference on Electrical Machines and Systems (ICEMS), Sydney, NSW, Australia, 2017, pp. 1-6.

- [54] M. Yousefian, H. A. Zarchi, S. Abdi and H. Gorginpour, "Optimal Design Parameter Determination for Brushless Doubly Fed Induction Machines," *International Conference on Electrical Machines (ICEM)*, Valencia, Spain, pp. 1716-1722, 2022.
- [55] S. Tohidi, P. Tavner, R. McMahon, H. Oraee, M. R. Zolghadri, S. Shao, and E. Abdi, "Low Voltage Ride-Through of DFIG and Brushless DFIG: Similarities and Differences", *Electric Power System Research*, vol. 110, pp. 64–72, May 2014.
- [56] E. Levi, M. Sokola, A. Boglietti, and M. Pastorelli, "Iron Loss in Rotor-Flux-Oriented Induction Machines: Identification, Assessment of Detuning, and Compensation," *IEEE Transaction on Power Electronics*, vol. 11, no. 5, pp. 698-709, Sep. 1996.
- [57] Y. Zeng, M. Cheng, X. Wei, and L. Xu, "Dynamic Modeling and Performance Analysis with Iron Saturation for Dual-Stator Brushless Doubly-Fed Induction Generator," *IEEE Transaction on Energy Conversion*, vol. 35, no. 1, pp. 260-270, March 2020
- [58] A. Accetta, F. Alonge, M. Cirrincione, M. Pucci, and A. Sferlazza, "Feedback Linearizing Control of Induction Motor Considering Magnetic Saturation Effects," *IEEE Transaction on Industry Applications*, vol. 52, no. 6, pp. 4843–4854, Nov. 2016.
- [59] M. A. Salahmanesh, H. Abootorabi Zarchi and H. Mosaddegh Hesar, "A Non-Linear Technique for MTPA-Based Induction Motor Drive Considering Iron Loss and Saturation Effects," *11th Power Electronics, Drive Systems, and Technologies Conference (PEDSTC)*, Tehran, Iran, pp. 1-6, 2020.
- [60] M. Pucci, "State-Space Space-Vector Model of the Induction Motor Including Magnetic Saturation and Iron Losses," *IEEE Transaction on Industry Applications*, vol. 55, no. 4, pp. 3453-3468, July-Aug. 2019.
- [61] O. Kiselychnyk, M. Bodson, and J. Wang, "Comparison of Two Magnetic Saturation Models of Induction Machines and Experimental Validation," *IEEE Transaction on Industrial Electronics*, vol. 64, no. 1, pp. 81–90, Jan. 2017.



Mohammad-Ali Salahmanesh received the M.Sc. degree from Ferdowsi University of Mashhad, Iran, in 2019 (with honors). He is currently working toward the Ph.D. degree in electrical machines and drives at Ferdowsi University of Mashhad, Iran. His research interests include control of electric drives, nonlinear control, modeling of electrical machines and power electronics.



Salman Abdi (M'21-SM'23) received the BSc degree from Ferdowsi University, Mashhad, Iran in 2009, the MSc degree from Sharif University of Technology, Tehran, Iran in 2011, both in electrical engineering, and the PhD degree in electrical machines design and optimisation from Cambridge University, UK in 2015. He is currently an Assistant Professor in electrical engineering with the University of East Anglia, Norwich, UK. His research interests revolve around electrical machine design, modelling, and instrumentation for renewable power generation and electric propulsion systems.



Richard McMahon received the degrees of BA (in Electrical Sciences) and PhD from Cambridge University in 1976 and 1980 respectively. Following postdoctoral work on semiconductor device processing, he became a University Lecturer in electrical engineering in 1989 with the Engineering Department, University of Cambridge, where he was a Senior Lecturer in 2000. Since 2016, he is with the Warwick Manufacturing Group, University of Warwick, Coventry, UK, as a Professor of Electrical Power Conversion. His current research interests include electric machines and power electronics.



Hamidreza Mosaddegh-Hesar received the Bachelor's, Master's and Ph.D. degrees in electrical engineering from Ferdowsi University of Mashhad, Mashhad, Iran, in 2011, 2014, and 2019, respectively. He is currently working as a Postdoctoral Fellow at Power and Energy Conversion Laboratory, University of Saskatchewan, Saskatoon, Canada. He serves as an Associate Editor for *IEEE Transactions on Industry Applications*.



Xiaodong Liang (M'06–SM'09) was born in Lingyuan, Liaoning, China. She received the B.Eng. and M.Eng. degrees from Shenyang Polytechnic University, Shenyang, China in 1992 and 1995, respectively, the M.Sc. degree from the University of Saskatchewan, Saskatoon, Canada in 2004, and the Ph.D. degree from the University of Alberta, Edmonton, Canada in 2013, all in electrical engineering.

From 1995 to 1999, she served as a lecturer at Northeastern University, Shenyang, China. In October 2001, she joined Schlumberger (SLB) in Edmonton, Canada, and was promoted to a Principal Power Systems Engineer with this world's leading oil field service company in 2009; she worked with Schlumberger for almost 12 years until August 2013. From 2013 to 2019, she was with Washington State University in Vancouver, WA, United States and Memorial University of Newfoundland in St. John's, NL, Canada as an Assistant Professor and later an Associate Professor. In July 2019, she joined the University of Saskatchewan in Saskatoon, Canada, where she is currently a Professor and Canada Research Chair in Technology Solutions for Energy Security in Remote, Northern, and Indigenous Communities. She was an Adjunct Professor with Memorial University of Newfoundland from 2019 to 2022. Her research interests include power systems, renewable energy, and electric machines.

Dr. Liang is a registered Professional Engineer in the province of Saskatchewan, Canada, a Fellow of IET, and Deputy Editor-in-Chief of *IEEE Transactions on Industry Applications*.